Journal of Catalysis **205,** 97–106 (2002)
doi:10.1006/jcat.2001.3390, available online at http://www.idealibrary.com on IDEAL®

Active Sites Characterization in Mixed Vanadium and Iron Antimonate Oxide Catalysts for Propane Ammoxidation

H. Roussel,* B. Mehlomakulu,† F. Belhadj,* E. van Steen,† and J. M. M. Millet*,[1]

*Institut de Recherches sur la Catalyse, CNRS, associé a l'Université Claude-Bernard, Lyon I, 2 avenue A. Einstein, F-69626 Villeurbanne Cedex, France; and †Catalysis Research Unit, Department of Chemical Engineering, University of Cape Town, Rondebosch 7701, South Africa

Received May 21, 2001; revised October 15, 2001; accepted November 1, 2001

Ammoxidation of propane was investigated over FeVSbO mixed oxide catalysts. The results obtained show that in $VSbO_4$ mixed oxide catalyst systems, substitution of vanadium by small quantities of iron has a strongly positive effect on the activity of the catalysts. With such a system, the selectivity to acrylonitrile decreases while the selectivity to propene increases. At high levels of vanadium substitution by iron, the activity was low but the selectivity towards acrylonitrile was enhanced. The characterization of the catalysts carried out using several techniques, such as X-ray diffraction, Mössbauer spectroscopy, X-ray absorption, and electron microscopy, has shown that a continuous solid solution was formed between $VSbO_4$ and $FeSbO_4$. At low iron loading, Fe^{3+} substituted for V^{4+} in the cationic-deficient structure $V^{4+}_{0.64}V^{3+}_{0.28}Sb^{5+}_{0.92}\diamond_{0.16}O_4$, leading to a structure with both cationic and anionic vacancies, $Fe^{3+}_{x}V^{3+}_{0.33}V^{4+}_{0.41-x}Sb^{5+}_{0.92}\diamond_{0.18}O_{4-x}$, and generating very active sites for alkane activation. At high iron loading, only V^{3+} was present in the bulk of the solids and only Fe^{3+} contributed to the isolation of the vanadium sites, which are selective to acrylonitrile. © 2002 Elsevier Science

Key Words: **acrylonitrile; propane ammoxidation; vanadium antimonate; iron antimonate; catalytic sites.**

1. INTRODUCTION

The process for production of acrylonitrile from propane instead of propene as feedstock has developed to the pilot plant stage. It is accepted that it will likely achieve the industrialisation step within the next few years. A modified VSbO system as a major candidate catalytic system has been extensively studied and the outcome is the existence of both numerous patents and publications (1). All these studies have contributed to the comprehensive knowledge we have today regarding these catalysts, including the identification of the active phase.

The $VSbO_4$ phase has been shown to be the active phase of this system (2). Isolation and dispersion of the vanadium site at the surface of this phase has been recognised as the key factor required for achieving high activity and, most important, high acrylonitrile selectivity (3, 4). In parallel to these studies, the effect of various additives has been investigated; especially studied are the Al and group VIb transition metals, which have been shown to enter in the active-phase structure (5–8). The hypothesis is that they contribute to the isolation of the vanadium site in the catalyst, thus improving the selectivity towards acrylonitrile. Al, when added in large quantities ($Al/(Al + Sb + V) > 0.5$), also plays a role as a support, owing to the formation of Al_2O_3. The group VIb transition metals, Cr, Mo, and W, which were shown to be effective promoters, are believed to act by providing active sites for the consecutive transformation of propylene to acrylonitrile, leading to more selective catalysts (6). Niobium, under specific conditions, may substitute for vanadium, but forms a new phase $SbNbO_4$ that is reported to have a positive effect on the catalytic properties (7). More recently, titanium has been studied as substituent to vanadium (8). It was shown that titanium decreases the activity of the catalysts but increases the selectivity to acrylonitrile. Such an effect was explained by isolation of the vanadium centres in the active phase, which led to a decrease in V–O–V moieties. These have been identified as centres responsible for degradation of propane and propylene; it was further proposed that the activity could be correlated with the content of V^{3+} in the unit cell of the active phase, whereas the selectivity to acrylonitrile could be correlated to the V^{4+}/V^{3+} ratio. If the latter model was in agreement with the role of Sb^{5+} proposed earlier in the activation of ammonia (9, 10), the principal role attributed to V^{3+} in the activation of the propane molecules could appear questionable. Although a recent publication stressed that V^{3+} may have an effect on the enhancement of the activity of an alkane molecule (11), most of the studies attribute this role to the V^{4+} or V^{5+} centres (12).

The objective of this work was to try to understand the role of vanadium and its environment in the activation of propane. To address this issue, we studied the effect of iron substitution to vanadium in the $VSbO_4$ active phase.

[1] To whom correspondence should be addressed. Fax: 33/472445399.

0021-9517/02 $35.00

The rationale behind this choice was the following: (i) the substitution of vanadium by iron will lead to the formation of a solid due to the fact that $FeSbO_4$ crystallises with the same type of structure as $VSbO_4$ (13) and that Fe^{3+} has the same cationic radii as V^{3+} (14); (ii) prepared in air, $VSbO_4$ contains a large amount of V^{4+}, which is balanced in the structure by cationic vacancies, leading to the approximate composition $V^{4+}_{0.64}V^{3+}_{0.28}Sb^{5+}_{0.92}\diamond_{0.16}O_4$(15); and (iii) the substitution will have a direct effect on the V^{4+}/V^{3+} ratio and valuable data would possibly be generated to correlate the activity and the selectivity in acrylonitrile to given species or compositions.

Furthermore, a kinetic scheme has been proposed in which acrylonitrile is formed both from propane directly and via a propylene intermediate (16). The existence of the latter pathway has recently been questioned (17), and further analyses performed in this study on VFeSbO catalysts allowed us to review and substantiate this discussion. Finally, $FeSbO_4$ is known to be an efficient catalyst for the ammoxidation of propene (18), and the presence of iron could thus change the selectivity pattern obtained over $VSbO_4$.

2. EXPERIMENTAL

The $V_{1-x}Fe_xSbO_4$ catalysts have been prepared using two different procedures, depending on their relative composition in vanadium and iron. Fe-rich compounds ($x > 0.6$) have been prepared according to a procedure described for $FeSbO_4$ (19), and V-rich compounds ($x < 0.5$) according to a procedure described for $VSbO_4$ (20). Briefly, in the first case, $Fe(NO_3)_3 \cdot 9H_2O$ was heated to 353 K, and Sb_2O_3 and NH_4VO_3 were then added under stirring. The solution was neutralized using NH_4OH, filtered and dried at 383 K for 24 h. The resulting solid was then calcined in air at 773 K for 20 h and at 1173 K for 2 h. In the second case, Sb_2O_3 was added to a NH_4VO_3 and $Fe(NO_3)_3 \cdot 9H_2O$ solution, and the resulting mixture was then heated under reflux and stirring for 18 h. The solution was then evaporated and the resulting slurry dried at 353 K before calcination at 623 and 973 K for 3 h each. The catalysts are designated according to their relative vanadium and iron contents.

The chemical compositions of the prepared solids were determined using atomic absorption and their surface area measured using nitrogen adsorption, according to the Brunauer–Emmett–Teller BET method. The step-scanned X-ray powder diffraction patterns were recorded at room temperature with 0.02° (2θ) steps over the 10–88° (2θ) angular range for 10 s counting time per step, using a Siemens D500 diffractometer and filtered Cu$K\alpha$ radiation. The data obtained from the powder patterns have been used to calculate the unit cell of the compounds using a method proposed by De Wolff (21). ^{57}Fe Mössbauer spectroscopy was performed at 298 K with a time-mode spectrometer and a constant acceleration drive. 2 GBq ^{57}Co/Rh was used as a radiation source. The hyperfine parameters were determined by computer fitting with a precision of about 0.02 mm $\cdot$ s^{-1}. In order to avoid too high a Mössbauer absorption, the samples were diluted in Al_2O_3 and pressed into pellets.

V–K edge X-ray absorption near-edge (XANES) spectra were collected at the LURE synchrotron facility in Orsay (D44) with a varying energy step of 1 eV/s in the range 5420–5450, 0.3 eV/2 s in the range 5450–5490, and 0.6 eV/s in the range 5490–5560, with three scans per sample. A Si(311) double-crystal monochromator was used for energy selection. To compare the different XANES spectra, the absorption background was first carried out using a linear law over the entire range, and the spectra were normalized in the middle of the first EXAFS oscillation, at ca. 80 eV above the absorption edge.

High-resolution electron microscopy was performed with a JEM equipped with an EDS LINK-ISIS (spatial resolution, 1 nm). Energy-dispensive X-ray (EDX) analyses were conducted using a probe size of 25 nm to analyse grains either isolated or sticking to each other. Diffuse reflectance fourier transform (DRIFT) spectra were recorded using a Magna-IRTM550 spectrometer from Nicolet between 4000 and 650 cm^{-1} with a 1-cm^{-1} precision. Samples were sieved between 200 and 300 μm before analysis.

X-ray photoelectron spectroscopy (XPS) measurements were performed with a VG ESCALAB 200 R. Binding energies were corrected relative to the carbon 1s signal at 284.6 eV. For quantitative analysis, the signal intensities of Fe 2p, V $2p_{3/2}$, Sb $3d_{3/2}$, and O 1s were measured using integrated areas under the detected peak. The O 1s and Sb $3d_{3/2}$ peaks being superposed, the O 1s signal intensity was obtained by subtraction of the calculated Sb $3d_{5/2}$ signal intensity to the total intensity of the peak. Results, expressed in terms of elemental ratios, were calculated with an experimental precision around 10%.

Catalytic activity measurements were conducted at atmospheric pressure in a dynamic differential microreactor containing 0.5–1.0 g of catalyst between 723 and 773 K. Reaction conditions were as follows: total flow rate, 17.2 cm$^3\cdot$min^{-1}; O_2/propane/NH_4/N_2/Ne = 1/2/2/7/0.05 (Ne was used as an internal standard). The catalysts were compared at 753 K using these conditions, with different masses to keep a comparable conversion level of about 18%. Acetonitrile (ACE), cyanhydric acid (HCN), propene (PRO), CO, and CO_2 were the by-products formed with acrylonitrile (ACN) under the reaction conditions used. The gas-feed composition was fixed using Brooks mass flow controllers, and the reactor was placed in a furnace controlled by a temperature programmer controller. The apparatus contained only stainless steel, except the reactor was in quartz. The powdered catalyst was on a sintered glass, and a little abyss on the surface of the glass reactor allowed placement of a thermocouple in the catalyst bed to measure the

reaction temperature. The gas mixture sampled before or after the reactor flowed to a six-way valve that then allowed injection on-line to a CP9003 CHROMPACK gas chromatography equipped with a thermal conductivity detector (TCD) and two columns in series (Tamis 5A and Haysep Q). The steam selection system and the tubes from the valves to the chromatographs were maintained at 403 K in order to avoid the polymerization and possible condensation of the products. The sample was first injected on the Haysep Q using a 10-way valve system. Before the peak of air reached the Tamis 5A column, the columns were switched so that the Tamis 5A could see and separate the permanent gases and CO only after they passed the Haysep Q again.

The conversion c was calculated using

$$c = \sum_n \frac{n[c_n]}{3[c_{\mathrm{PRO}}]} \times 100\%, \qquad [1]$$

where n is the number of carbon in the product c_n, $[c_n]$ is the molar concentration of products with n carbon atoms, and $[c_{\mathrm{pro}}]$ is the molar concentration of a propane in feed.

The selectivity for a certain product is calculated on the basis of carbon efficiency using

$$s_{\mathrm{p}} = P\frac{[c_p]}{\sum_n c_n} \times 100\%, \qquad [2]$$

where c_p and c_n are the molar concentrations of a product with p and n carbons, respectively. In each case, the carbon balance was calculated and appeared to be equal to $100 \pm 2\%$.

3. RESULTS

3.1. Characterization of the Fresh and Used Catalysts

The results of the chemical analysis and BET surface area measurements are presented in Table 1. The Fe/(Fe + V) and (V + Fe)/Sb ratios obtained correspond to the theoretical values. The catalysts were not treated at the same temperature but it can be observed that the surface area of $VSbO_4$ increased with the iron substitution and that of $FeSbO_4$ decreased with the vanadium substitution. For the compound 60FeVSb, the effect of the heating temperature on the surface area was studied (Fig. 1). A strong decrease down to $2\,m^2 \cdot g^{-1}$ at 1173 K was observed. It was also shown that the surface areas did not vary under the conditions of catalytic testing.

TABLE 1

Chemical Analyses and BET Surface Area Measurements Data

Compound	Atomic weight (%) Fe	V	Sb	T (K)[a]	Surface area ($m^2 \cdot g^{-1}$)
VSb	—	21.5	49.5	973	3.3
10FeVSb	2.2	19.0	48.9	973	10.0
20FeVSb	4.2	16.8	48.9	973	16.0
40FeVSb	8.9	12.6	50.3	973	21.4
60FeVSb	15.2	8.9	49.5	973	20.5
80FeVSb	18.6	4.2	51.5	1173	6.6
90FeVSb	20.8	2.2	51.8	1173	8.3
FeSb	22.9	—	50.4	1173	10.7

[a] Temperature of heat treatment for the preparation.

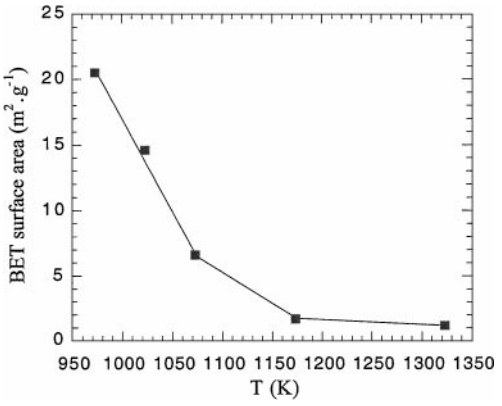

FIG. 1. Evolution of the BET surface area of the 60FeVSb compound as a function of the firing temperature.

The X-ray diffraction patterns of the solids are presented in Fig. 2. They all correspond to a single well-crystallised rutile-type phase. In stoichiometric rutile phase, iron and antimony have been shown to be randomly distributed in the cations sites (22), whereas vanadium and antimony undergo a partial ordering, leading to a 32-fold supercell with $2\sqrt{2}a, 2\sqrt{2}b, 4c$ (23). Because it was impossible to observe superlattice reflections in the X-ray powder diffraction patterns of the catalysts, we calculated the a and c parameters of the simple tetragonal unit cell (Table 2, Fig. 3). The a parameter increased progressively with the iron content of the $Fe_xV_{1-x}SbO_4$ solid solution, whereas the c parameter increased strongly between $x = 0$ and 0.5 and remained constant at higher iron content. In order to confirm that a solid solution existed in the vanadium-rich composition range, a study by electron microscopy with EDX analyses was conducted on the 20FeVSb catalyst. The solid particles were found to correspond to a single or aggregates of grains (10–20 nm) whose Fe/(Fe + V) and Fe/Sb atomic ratios were quantified (Fig. 4). Despite the large standard deviation obtained when atomic ratios were evaluated with this technique, we observed only a narrow compositional population with Fe/(Fe + V) and Fe/Sb mean ratios equal to 0.19 ± 0.03 and 0.22 ± 0.02, corresponding to the total cationic composition of the sample.

The surface composition of the catalysts has been determined by XPS before and after catalytic test (Table 3). The V (516.8 ± 0.2 eV), Sb (540.25 ± 0.10 eV), and Fe

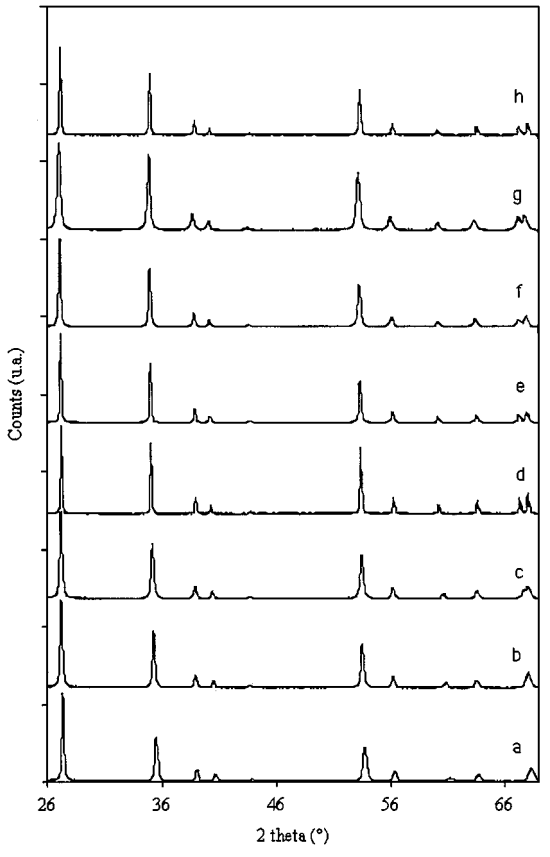

FIG. 2. X-ray diffraction patterns of the $Fe_xV_{1-x}SbO_4$ catalysts: (a) VSb, (b) 10FeVSb, (c) 20FeVSb, (d) 40FeVSb, (e) 60FeVSb, (f) 80FeVSb, (g) 80FeVSb, (h) FeSb.

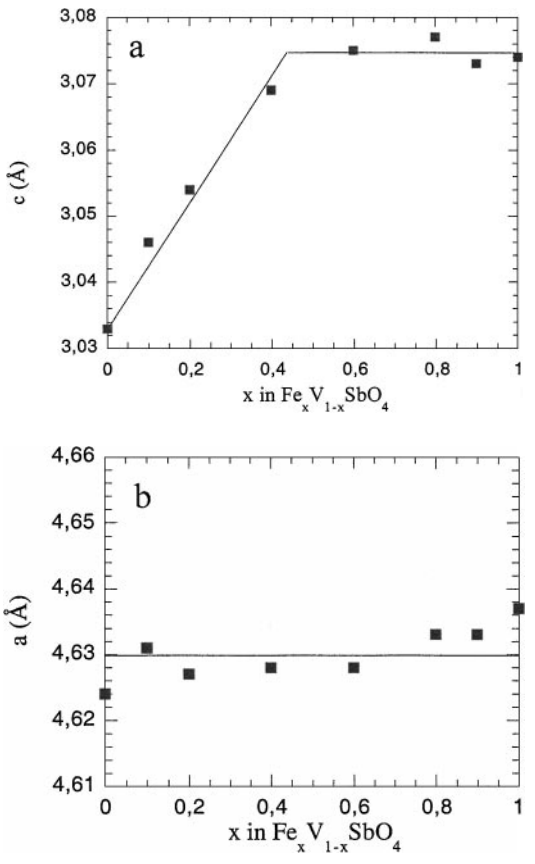

FIG. 3. Evolution of the unit cell parameters of the $Fe_xV_{1-x}SbO_4$ solid solution as a function of x.

(711.70 ± 0.15 eV) binding energies remained very constant in all the analyses and did not vary significantly before or after catalytic testing. For all the compounds, the surface iron content was consistently lower than the bulk content and the surface antimony content higher. After the catalytic test, the surface iron content of the samples increased to about the same as in the bulk. The surface antimony content remained constant except for the pure $VSbO_4$ compound, for which it strongly increased.

The V–K edge, XANES, and Mössbauer spectroscopy were used to characterise the average valence states of vanadium and iron in the compounds. The V–K edge of the VSb, 20FeVSb, and 60FeVSb samples along with that of the V^{4+} standard $(VO)_2P_2O_7$ phase are presented in Fig. 5. For the 60FeVSb sample, a single pre-edge peak at 5470.0 eV was observed, whereas for the VSb and 20FeVSb compounds, a second peak at 5469.2 eV was observed. These peaks have been attributed to V^{4+} and V^{3+} by comparison with standard phase and literature data (24). Results of fitting to a model with a weighted superposition of V^{4+} and V^{3+}components (Fig. 6) showed that the $V^{4+}:V^{3+}$ ratio obtained for VSb (63:37) was relatively close to the theoretical one calculated for the $V^{4+}_{0.64}V^{3+}_{0.28}Sb^{5+}_{0.92}\diamond_{0.16}O_4$ stoichiometry (70:30). The calculated $V^{4+}:V^{3+}$ ratio for

TABLE 2

Cell Parameters of the Tetragonal Rutile Phase Calculated for the $Fe_xV_{1-x}SbO_4$ Compounds

Cell parameters	x in $Fe_xV_{1-x}SbO_4$							
	0.0	0.1	0.2	0.4	0.6	0.8	0.9	1.0
a (Å)	4.624 (1)	4.631 (1)	4.627 (1)	4.6280 (9)	4.6278 (7)	4.6328 (7)	4.6329 (9)	4.637 (1)
c (Å)	3.0332 (8)	3.046 (1)	3.0543 (6)	3.0692 (5)	3.0752 (4)	3.0772 (4)	3.0737 (5)	3.0737 (7)

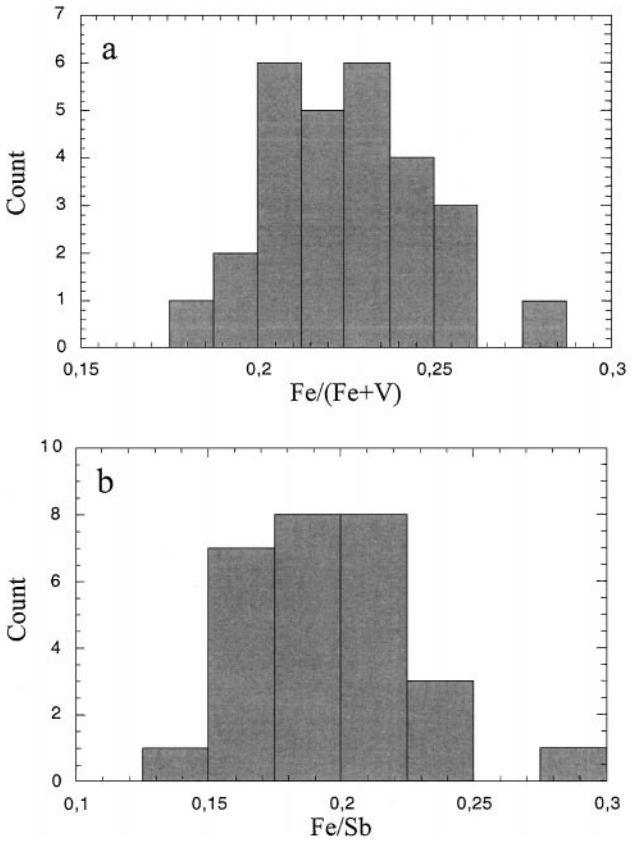

FIG. 4. Histogram of X-ray microanalysis results of 20FeVSb.

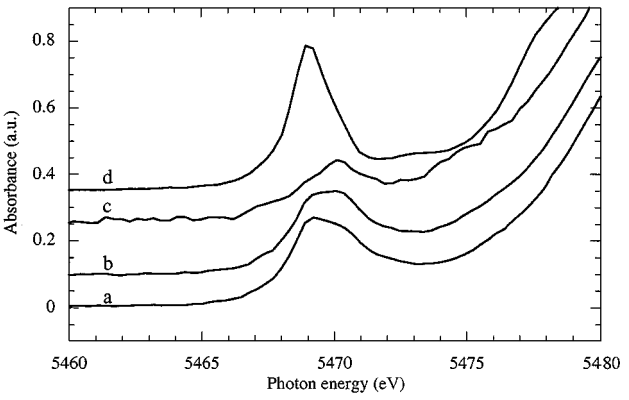

FIG. 5. Normalised V–K edge XANES spectra of (a) VSb, (b) 20FeVSb, (c) 60FeVSb, (d) $(VO)_2P_2O_7$.

the 20FeVSb compound was 53 : 47, indicating either an increase in the V^{3+} content or a decrease in the V^{4+} content. The data obtained did not exclude the presence of V^{5+} in the sample, which would have been characterised by a peak in a range in energy close to that attributed to V^{3+}. In the 60FeVSb compound, only V^{3+} ions were present.

The ^{57}Fe Mössbauer spectra of the samples were fitted with one ferric doublet (Fig. 7). The calculated parameters reported on Table 4 corresponded to those published for $FeSbO_4$ (25, 26). This doublet is caused by paramagnetic Fe^{3+} ions, of which the isomer shifts (δ) and quadrupolar splittings (Δ) at room temperature are typical of Fe^{3+} (high spin) in octahedral coordination. The high value of Δ accounts for a relatively high electrical gradient field at the iron nucleus, which should arise both from a distortion of the octahedra formed with the nearest oxygen neighbors and from the lack of a strict ordering of the cations. The Mössbauer parameters of the solids after catalytic testing were the same as before, showing that

TABLE 3

Atomic Surface Composition of the Solids Calculated from XPS Analyses Data

	Fe/(Fe + V)		Sb/(V + Fe)	
Compound	Before test	After test	Before test	After test
VSb	0.00	0.00	1.3	2.5 (1.0)
10 FeVSb	0.04	0.08 (0.10)	1.1	1.4 (1.0)
20 FeVSb	0.10	0.22 (0.20)	1.3	1.2 (1.0)
40 FeVSb	0.30	0.39 (0.40)	1.5	1.5 (1.0)
60 FeVSb	0.52	0.55 (0.61)	1.9	2.0 (1.0)
80 FeVSb	0.85	0.77 (0.81)	1.6	1.5 (1.0)
FeSb	1.00	1.00	1.3	1.1 (1.0)

Note. Bulk compositions calculated from chemical analyses are given in parentheses for comparison.

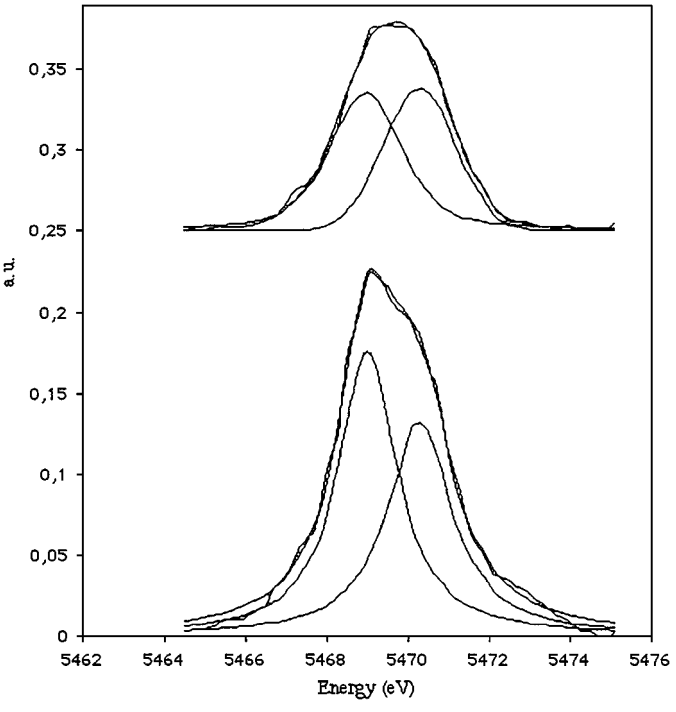

FIG. 6. Fitting of the pre-edge peak of the normalised V–K edge XANES spectra of VSb (top) and 20FeVSb (bottom) compounds.

TABLE 4

Mössbauer Parameters Computed from the Spectra of the $Fe_xV_{1-x}SbO_4$ Samples Recorded at 295 K and Fitted to One Doublet

Compound	δ	W ($mm \cdot s^{-1}$)	Δ
20FeVSb	0.35	0.40	0.69
40FeVSb	0.34	0.39	0.69
60FeVSb	0.34	0.39	0.71
80FeVSb	0.34	0.40	0.72
FeSb	0.34	0.39	0.73
20FeVSb after test	0.36	0.39	0.69
60FeVSb after test	0.34	0.38	0.71

Note. δ, Isomer shift (referred to αFe); W, line width; Δ, quadrupolar splitting.

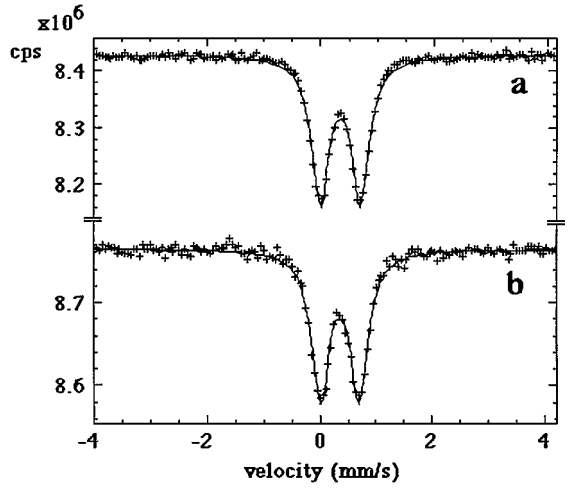

FIG. 8. Experimental Mössbauer spectra of the 20FeVSb catalyst, recorded at 295 K before (a) and after (b) catalytic testing. Solid lines are derived from least-square fits.

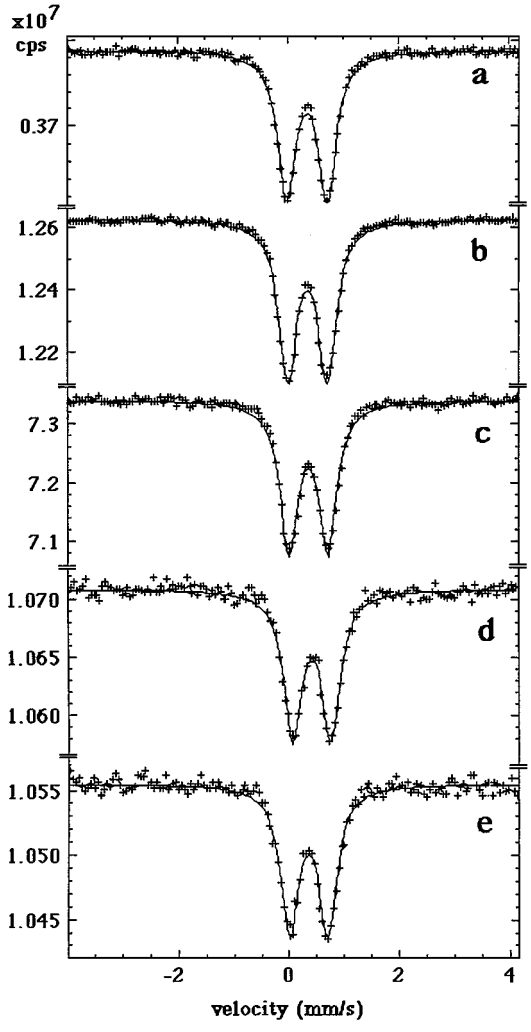

FIG. 7. Experimental Mössbauer spectra of the $Fe_xV_{1-x}SbO_4$ catalysts, recorded at 295 K. Solid lines are derived from least-square fits. (a) FeSb, (b) 80FeVSb, (c) 60FeVSb, (d) 40FeVSb, (e) 20FeVSb.

iron was not reduced in the testing conditions (Table 4, Fig. 8).

The DRIFT spectra of the vanadium-rich catalysts showed two bands, at 1015 and 880 cm^{-1} (Fig. 9). The observed bands confirmed the presence of cationic vacancies, as they correspond precisely to those reported for the $VSbO_4$ structure in literature (15, 27).

3.2. Catalytic Properties of the Catalysts

The catalytic properties of the $Fe_xV_{1-x}SbO_4$ compounds have been compared in the ammoxidation of propane at almost iso-conversion, and at 753 K under the conditions described in the experimental section (Table 5). The products

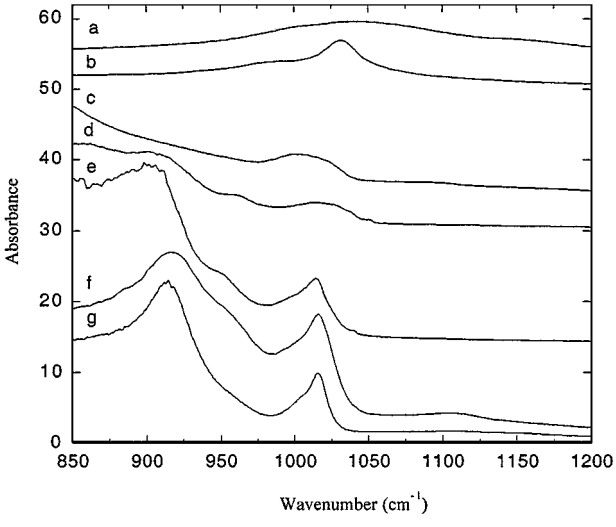

FIG. 9. DRIFT spectra of the catalysts: (a) FeSb, (b) 80FeVSb, (c) 60FeVSb, (d) 40FeVSb, (e) 20FeVSb, (f) 10FeVSb, (g) VSb.

TABLE 5

Catalytic Properties of the Compounds $Fe_xV_{1-x}SbO_4$ in the Ammoxidation of Propane at 753 K

Compound	RC_3 (10^{-8} mol · s^{-1} · m^{-2})	Conversion (%)	Selectivities (%)					
			CO	CO_2	PRO	HCN	ACE	ACN
VSb	57.7	16	11	10	33	16	6	24
10FeVSb	129.3	17	11	8	49	14	6	12
20FeVSb	136.7	19	8	7	51	13	6	15
40FeVSb	58.1	18	13	14	28	16	5	24
60FeVSb	21.0	22	13	14	20	16	4	33
80FeVSb	15.6	19	15	17	11	17	2	38
FeSb	9.6	22	4	67	14	4	0	11

Note. ACE, acetonitrile; ACN, acrylic acid; RC_3, rate of transformation of propane.

obtained from the catalysts studied were PRO, CO, CO_2, HCN, ACE, and ACN. The results are presented in Figs. 10 and 11. The results are expressed as the observed transformation rate of propane per unit surface area of catalyst and selectivities toward the products that are listed above. It can be observed that the activity of the $Fe_xV_{1-x}SbO_4$ compounds strongly increased with the iron content to approximately $x = 0.15$; beyond this value it significantly decreased to around $x = 0.4$ and then increased slightly to $x = 1$. However, the selectivity to propene increased and that to ACN and CO_x decreased slightly when the activity increased strongly and further, respectively, decreased and increased strongly when the activity decreased. Typically, $FeSbO_4$ catalytic has a different behavior with a significantly lower activity and a high selectivity to CO_x.

4. DISCUSSION

The results obtained in this study showed that the substitution of iron for vanadium in $VSbO_4$ led to a continuous solid solution between $VSbO_4$ and $FeSbO_4$. Chemical analysis data allowed us to calculate the composition of the compounds assuming the presence of a rutile phase with four oxygens per formula (Table 6). The cation-deficient composition of $VSbO_4$, characterised earlier (15), was confirmed. The total formula was consistent with the data obtained using XANES, validating the technique as beneficial for evaluating the $V^{4+}:V^{3+}$ ratio. In the catalysts with a low iron content, it was not possible to calculate a composition on the basis of a fully oxidized rutile structure. The charge discrepancy introduced by the iron substitution could be balanced by the presence of V^{5+} or anionic vacancies. In the first case, V^{5+} and V^{3+} would not have been differentiated in the XANES data and the $V^{4+}:V^{3+}$ ratio observed should have been 38 : 62, which is far from what was really observed. A phase composition with anionic vacancies appeared more probable (Table 6). These vacancies were present in the solid when x in $Fe_xV_{1-x}SbO_4$ varied between 0 and 0.6. A continuous decrease in the V^{4+} content was observed in this range of composition (Fig. 12). Both the cationic and anionic vacancy contents passed through a maximum around $x = 0.15$ (Fig. 13). These transformations

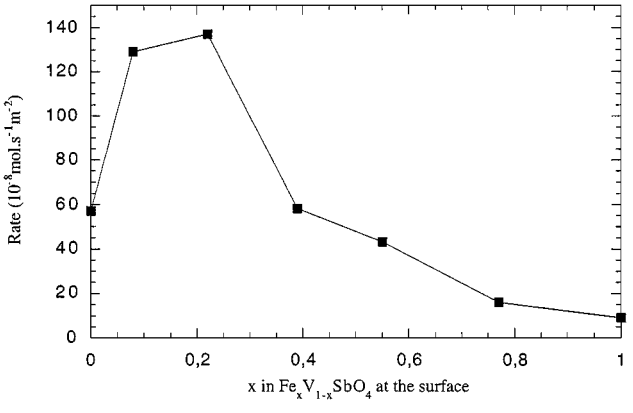

FIG. 10. Variation of the rate of propane conversion at 753 K as a function of the surface iron composition of the $Fe_xV_{1-x}SbO_4$ catalysts.

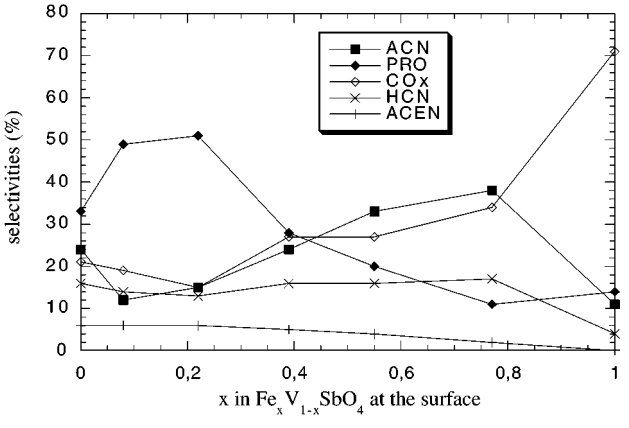

FIG. 11. Variation of the selectivities at 753 K as a function of the surface iron composition of the $Fe_xV_{1-x}SbO_4$ catalysts.

TABLE 6

Calculated Formula of the Compounds Using all the Characterisation Data

Compound	Calculated formula
VSb	$V^{3+}_{0.27}V^{4+}_{0.66}\diamond_{0.16}Sb^{5+}_{0.91}O_4$
10FeVSb	$Fe^{3+}_{0.09}V^{3+}_{0.32}V^{4+}_{0.52}\diamond_{0.18}Sb^{5+}_{0.92}O_{3.95}$
20FeVSb	$Fe^{3+}_{0.18}V^{3+}_{0.33}V^{4+}_{0.41}\diamond_{0.16}Sb^{5+}_{0.92}O_{3.88}$
40FeVSb	$Fe^{3+}_{0.38}V^{3+}_{0.34}V^{4+}_{0.23}\diamond_{0.10}Sb^{5+}_{0.95}O_{3.92}$
60FeVSb	$Fe^{3+}_{0.63}V^{3+}_{0.40}Sb^{5+}_{0.97}O_4$
80FeVSb	$Fe^{3+}_{0.80}V^{3+}_{0.19}Sb^{5+}_{1.01}O_4$
90FeVSb	$Fe^{3+}_{0.90}V^{3+}_{0.10}Sb^{5+}_{1.01}O_4$
FeSb	$Fe^{3+}_{0.99}Sb^{5+}_{0.99}O_4$

should account for the observed change in cell parameters of the structure that should correspond to the $VSbO_4$ 32-fold supercell, within the same range of composition. At higher iron content, a rutile structure with only V^{3+} cations and almost no vacancies was observed. No significant variations in the cell parameters were observed, fitting with the fact that Fe^{3+} and V^{3+} cations have similar ionic size. The presence of cationic vacancies was confirmed by the observation of bands at 1015 and 880 cm^{-1} in the DRIFT spectra. Moreover, the linear relationship previously shown to exist between the intensity of the band at 1015 cm^{-1} and the number of cationic vacancies (15) was observed (Fig. 14).

The results clearly showed that at low levels of vanadium-by-iron substitution, Fe^{3+} was substituting not V^{3+} but V^{4+}. The positive charge defect relative to this substitution was balanced by the creation of anionic vacancies, while the number of cationic vacancies remained at best constant or even slightly increased. The rutile structure is made of edge-sharing octahedra connected together and forming chains in the [001] direction. To be balanced by cationic

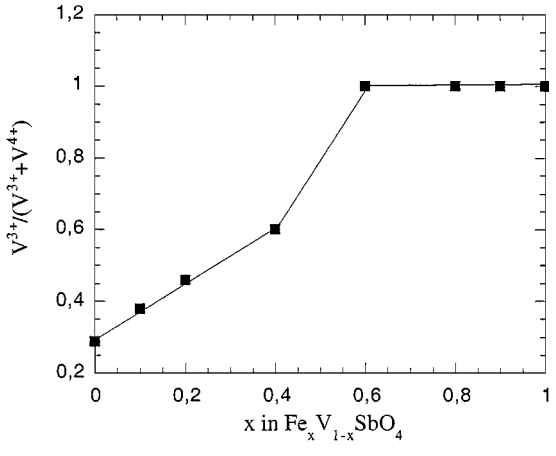

FIG. 12. Variation of the $V^{3+}/(V^{3+}+V^{4+})$ as a function of the iron composition of the $Fe_xV_{1-x}SbO_4$ catalysts.

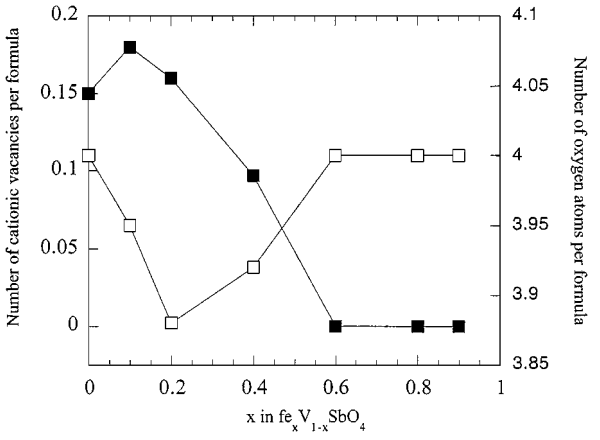

FIG. 13. Variation of the cationic vacancies content and of the number of oxygen atoms per formula as a function of the iron composition of the $Fe_xV_{1-x}SbO_4$ catalysts.

vacancies, V^{4+} should form locally in these chains positively charged defects that could correspond to two V^{4+} octahedra sharing an edge. This is consistent with the increase in the *c* parameter observed when the V^{4+} content decreased (for $0 \leq x \leq 0.6$ in $Fe_xV_{1-x}SbO_4$). Two of these pairs would be associated with a cationic vacancy. Since 0.64 V^{4+} were present per formula in the pure vanadium antimonate (Table 6), this corresponds to 0.16 defects. Taking into account the fact that this defect number was approximately the same as that of the maximum substitution of V^{4+} by Fe^{3+}, one may propose that only one out of the four V^{4+} cations could be substituted without destabilising the defect.

At low iron content, the substitution of vanadium by iron cations in the vanadium antimonate was shown to have a strong effect on the activity of the catalyst (Table 5). Such an

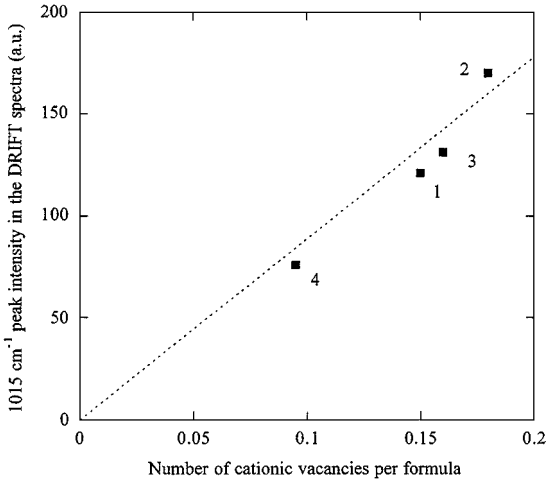

FIG. 14. Variation of the intensity of the DRIFT band at 1015 cm^{-1} as a function of the number of cationic vacancies per $Fe_xV_{1-x}SbO_4$ formula. (1) $x = 0$, (2) $x = 0.1$, (3) $x = 0.2$, (4) $x = 0.4$.

effect could not be attributed to the Fe^{3+}/Fe^{2+} redox couple, since Fe^{2+} was detected neither before nor after catalytic testing. Therefore, it can be inferred that the Fe^{3+}/Fe^{2+} redox couple is not involved in the reaction mechanism. This leads to a first conclusion, that trivalent cations like Al^{3+}, present in the industrial catalysts, could replace Fe^{3+} and give the same effect. The increase in activity could neither be attributed to the supra surface antimony sites detected by XPS because no relation could be observed between the antimony to iron and vanadium ratio of the surface and the activity nor to the selectivity of the catalysts. Moreover, all the effects reported for these supra surface antimony sites concern the selectivity but never the activity of the catalysts (20, 27, 28). The increase in activity appears to be related to the formation of the new defect structure that creates highly active sites for the activation of propane. These sites, however, were less selective towards ACN.

The initial activation step of the alkane has been described as a two-step mechanism with first a C–H bond cleavage that may take place via the attack by a positive electron hole leading to a radical (29):

$$C_3H_8 + p^+ \leftrightarrow C_3H_7^{\bullet} + H^+.$$

Since an electron hole can be filled by an electron hopping from a neighbour anion ($O^{2-} + p^+ \leftrightarrow O^-$), the above equation may be written as

$$C_3H_8 + O^- \leftrightarrow C_3H_7^{\bullet} + (O^{2-})^{o} + H^+,$$

where $(O^{2-})^{o}$ is an oxygen anion in its normal lattice position (neutral). The formed radical can be subsequently transformed into an alkoxide ion using an electron trapped at an oxide vacancy (30),

$$C_3H_7^{\bullet} + V_O^{\bullet} + (O^{2-})^{o} \rightarrow (OC_3H_7)^-_{ads} + V_O^{\bullet\bullet},$$

where $V_O^{\bullet}$ and $V_O^{\bullet\bullet}$ represent, in the Kröger–Vink notation for point defects in crystals, oxygen vacancies with effective charges +1 and +2.

The direct abstraction of an H^- from an anionic vacancy has also been proposed (31). In such an environment, both charge transfer reactions should occur preferentially at defect sites which are different for the two steps (i.e., cationic and anionic vacancies) and which are usually not present simultaneously in large amounts in the same structure. We postulate that the presence of both types of defect in close vicinity is a key factor in the activity of iron-substituted vanadium antimonate. The presence of cationic vacancies is related to that of V^{4+}, which may also be involved through charge transfer in the formation of active species for the first step, $V^{4+} + O^{2-} \leftrightarrow V^{3-} + O^-$, whereas anionic vacancies may be involved through another charge transfer in the formation of active species for the second step, $V^{3+} + V_o^{\bullet\bullet} \leftrightarrow V^{4+} + V_o^{\bullet}$. The concomitant increase in propene selectivity with the substitution of vanadium at low iron content should be due to the presence of the anionic vacancies, which limits the number of active oxygen species for the further transformation of the intermediate formed and to the decrease of the nucleophilic character of the oxygen cations of the defect structure related to the anion deficiency. Concerning the selectivity to acetonitrile, its nonevolution in the range of catalyst compositions tested seems to support the postulate made earlier of a main pathway directly from propane for the formation of this product (32).

Because we postulated that the activity is related to the presence of defects, the less defect, the lower the activity should be. That is indeed observed with catalysts with higher iron content, in which the number of defects is low and for which the activity is strongly decreased (Table V). However, with such catalysts, the selectivity to acrylonitrile increased due to the dispersion of vanadium, which should allow statistically more reactions with the activated ammonia molecules. These results correlate well with those obtained by Nilsson *et al.*, who have shown that the more selective catalytic sites were isolated vanadium centres (5). The results obtained also showed that iron played a role in stabilising the surface composition in the conditions of the catalytic tests, partially avoiding the formation of surface antimony oxide, SbO_x. In the absence of iron, the vanadium antimonate catalyst surface equilibrates with the reductive reaction atmosphere by the reduction of Sb^{5+} into Sb^{3+}. Since Sb^{3+} cannot be stabilised in the rutile structure, SbO_x is formed at the surface. In iron-containing vanadium antimonate, the surface equilibrates differently by increasing the surface anionic vacancy content (i.e., the surface iron content) (Table III). It has been shown that antimony oxide is inactive in the reaction but that limited amounts of antimony oxide at the surface of the rutile phase promote the selectivity to acrylonitrile (33). Because iron limits the formation of antimony oxide at the surface, it is likely to lead to more efficient but less selective catalysts.

The question that remains is whether the oxidation state of the vanadium active sites is +4 or +3. In fact this question could be meaningless if it were the defects that played the main roles. In such case, it would be the V^{4+}/V^{3+} redox couple that would intervene in the electron transfers and the creation of the active sites; furthermore, in the two steps proposed for the alkane activation, the two different cations could be involved as proposed above. A similar mechanism cannot be excluded, and could well occur for $(VO)_2P_2O_7$-based catalysts (explaining why, in the literature, all the vanadium species have been proposed over the years as active sites). The presence of cationic vacancies at the surface has been proposed and related to both the presence of V^{5+} and the *p* type of the semiconductivity observed (34), whereas the presence of anionic vacancies could be partially related to that of V^{3+}.

5. CONCLUSION

The results obtained in this study have shown that the substitution of vanadium by iron in $VSbO_4$ led to a continuous solid solution from $VSbO_4$ to $FeSbO_4$. At low loading, iron-substituted V^{4+} in the cation-deficient structure of $VSbO_4$ and not V^{3+} as would have been expected. In such a case the resulting positive charge discrepancy is balanced by oxygen vacancies, leading to a structure with both cationic and anionic vacancies. $Fe_x^{3+}V_{0.33}^{3+}V_{0.41-x}^{4+}\diamond_{0.18}Sb_{0.92}^{5+}O_{4-x}$ is thus obtained with a maximum of vacancies in the range $0.1 \leq x \leq 0.2$. This structure led to catalytic sites with higher efficiency, able to activate propane but less selective to ACN. The presence in close vicinity of cationic and anionic vacancies should promote both the formation of radicals from the alkane molecules and their subsequent transformation into alkoxide intermediate species in the reaction network. The concomitant decrease in selectivity in acrylonitrile to the benefit of that in propene would be related to the decrease of the number of oxygen species that could be implicated in the further transformation of the intermediate alkoxide species. The results obtained also point to a possible role of iron cations in the stabilisation of the rutile structure by participating in a redox equilibration of the solid with a cationic diffusion process between bulk and surface.

At high loading, iron substitutes V^{3+} in a structure with less vacancy. It decreases monotonoically the activity but increases the selectivity to ACN, probably by isolating the active vanadium sites, as proposed earlier. We have also shown that the Fe^{3+}/Fe^{2+} redox couple was not directly involved in the reaction mechanism but that iron intervenes by changing the relative valence state of vanadium and the cationic and anionic assessment in the structure. Such a role could similarly be attributed to aluminum in the industrial catalysts.

ACKNOWLEDGMENT

Dr. V. Briois from LURE Synchrotron is gratefully acknowledged for her help and for fruitful discussions.

REFERENCES

1. Centi, G., Grasselli, R. K., Trifiro, F., *Catal. Today* **13**, 661 (1992).
2. Guttmann, A. T., Grasselli, R. K., and Brazdil, J. F., U.S. Patents 4,746,641 and 4,788,317 (1988).
3. Centi, G., and Mazzoli, P., *Catal. Today* **28**, 351 (1996).
4. Andersson, A., Andersson, S. L. T., Centi, G., Grasselli, R. K., Sanati, M., and Trifiro, F., *Appl. Catal*. **113**, 43 (1994).
5. Nilsson, J., Landa-Canovas, A. R., Hansen, S., and Andersson, A., *J. Catal.* **160**, 244 (1996).
6. Centi, G., Grasselli, R. K., Patane, E., and Trifiro, F., *Stud. Surf. Sci. Catal.* **55**, 515 (1990).
7. Mimura, Y., Ohyachi, K., and Matsuura, I., *Sci. Tech. Catal.* 69 (1998).
8. Wickman, A., Wallenberg, L. R., and Andersson, A., *J. Catal.* **194**, 153 (2000).
9. Centi, G., and Perathoner, S., *Appl. Catal.* **124**, 317 (1995).
10. Andersson, A., Andersson, S. L. T., Centi, G., Grasselli, R. K., Sanati, M., and Trifiro, F., *Appl. Catal.* **113**, 43 (1994).
11. Cavani, F., Ligi, S., Monti, T., Pierelli, F., Trifiro, F., Albonetti, S., and Mazzoni, G., *Catal. Today* **61**, 203 (2000).
12. Grzybowska-Swierkosz, B., *Appl. Catal. A* **157**, 409 (1997).
13. *Natl. Bur. Stand. (U.S.) Monogr.* **25**(19), 49 (1982).
14. Shannon, R. D., and Prewitt, C. T., *Acta Crystallogr. Sect. B* **25**, 925 (1969).
15. Landa-Canovas, A., Nilsson, J., Hansen, J. S., Stahl, K., and Andersson, A., *J. Solid State Chem.* **116**, 369 (1995).
16. Catani, R., Centi, G., Trifiro, F., and Grasselli, R. K., *Ind. Eng. Chem. Res.* **31**, 107 (1992).
17. Brazdil, L. C., Ebner, A. M., and Brazdil, J. F., *J. Catal.* **163**, 117 (1996).
18. van Steen, E., Schnobel, M., Walsh, R., and Riedel, T., *Appl. Catal. A* **165**, 349 (1997).
19. Allen, M., Betteley, R., Bowker, M., and Hutchings, G. J., *Catal. Today* **9**, 97 (1991).
20. Nilsson, R., Linblad, T., Andersson, A., Song, C., and Hansen, S., *Stud. Surf. Sci. Catal.* **82**, 281 (1994).
21. De Wolff, P. M., *J. Appl. Crystallogr.* **1**, 108 (1968).
22. Berry, F. J., Holden J. G., and Loretto, M. H., *J. Chem Soc., Faraday Trans.* **83**, 615 (1987).
23. Bauer, W. H., *Z. Kristallogr.* **209**, 143 (1994).
24. Ramanujachary, K. V., Sunstrom, J. E., Fawcett, I., Shuk, P., Greenblatt, M., Croft, M., Nowik, I., Herber, R. H., and Khalid, S., *Mater. Res. Bull.* **34**(5), 803 (1999).
25. Kriegsmann, H., Öhlmann, G., Scheve, J., and Ulrich, F. J., *in* "Proceedings, 6th International Congress on Catalysis, London, 1976" (G. C. Bond, P. B. Wells, and F. C. Tompkins, Eds.), Vol. 2, p. 836. The Chemical Society, London, 1977.
26. Berry, F. J., Holden, J. G., and Loretto, M. H., *J. Chem Soc., Dalton Trans.* **7**, 1727 (1987).
27. Nilsson, R., Lindblad, T., and Andersson, A., *J. Catal.* **148**, 501 (1994).
28. Centi, G., Perathoner, S., and Trifiro, F., *Appl. Catal. A* **157**, 143 (1997).
29. Herrmann, J. M., Vernoux, P., Béré, K., and Abon, M., *J. Catal.* **167**, 106 (1997).
30. Matsuura, I., Oda, H., and Oshida, K., *Catal. Today* **16**, 547 (1993).
31. Jalowiecki-Duhamel, L., Monnier, A., and Barbaux, Y., *J. Catal.* **176**, 285 (1998).
32. Minow, G., Schnabel, K. H., and Öhlmann, G., *React. Kinet. Catal. Lett.* **22**(3–4), 399 (1983).
33. Rizayev, R. G., Mamedov, E. A., Vistovskii, V. P., and Sheinin, V. E., *Appl. Catal.* **83**, 103 (1999).
34. Delichere, P., Béré, K., and Abon, M., *Appl. Catal. A* **172**, 295 (1998).